PAPER • OPEN ACCESS

Coupling of mesoscale Weather Research and Forecasting model to a high fidelity Large Eddy Simulation

To cite this article: C Santoni et al 2018 J. Phys.: Conf. Ser. 1037 062010

View the article online for updates and enhancements.

Related content

- Large eddy simulation of turbulent cavitating flows
- A Gnanaskandan and K Mahesh
- Quantifying variability of Large Eddy Simulations of very large wind farms S J Andersen, B Witha, S-P Breton et al.
- The Long distance wake behind Horns Rev I studied using large eddy simulations and a wind turbine parameterization in
- WRF
 O Eriksson, M Baltscheffsky, S-P Breton et

IOP Conf. Series: Journal of Physics: Conf. Series 1037 (2018) 062010 doi:10.1088/1742-6596/1037/6/062010

Coupling of mesoscale Weather Research and Forecasting model to a high fidelity Large Eddy Simulation

Santoni C, García-Cartagena EJ, Ciri U, Iungo GV and Leonardi S

Department of Mechanical Engineering, The University of Texas at Dallas. Texas, US.

E-mail: stefano.leonardi@utdallas.edu

Abstract. Numerical simulations of the flow in a wind farm in north Texas have been performed with WRF (Weather Research and Forecasting model) and our in-house LES code. Five nested domains are solved with WRF to model the meso-scale variability while retaining a resolution of 50 meters in the wind farm region. The computational domain of our in-house LES code is nested into the inner most domain of the WRF simulation from where we get the inlet boundary conditions. The outlet boundary conditions are radiative and at this stage the coupling between the two codes is one-way. The turbines in WRF are mimicked using a modified Fitch approach, while in our in-house LES we have used a rotating actuator disk combined with immersed boundaries for tower and nacelle. Numerical results agree well with meteorological data from the met tower. The power production obtained numerically on each turbine compares well with SCADA data with an index of agreement ranging between 80% to 90%. The power production from the numerical results of our in-house LES code is slightly closer to SCADA data than that of WRF.

1. Introduction

In order to increase wind energy capture, manufacturers are making larger rotors with diameters of the order of 200 m. This implies that loads and power production fluctuations are affected by the variability in the atmospheric boundary layer and meandering of coherent structures. A lot of work has been done in developing wind turbine models, such as the actuator line and disk models [1, 2], and quantifying the onset of vortex breakdown. Most of these studies use uniform or sheared inflow, with some synthetic turbulence, but do not account for variability of the flow field on large time scales. In fact, the resolution used for the turbine model is such that the computational domain is limited to the region in the immediate vicinity of the turbines.

On the other hand, wind turbine models such as that developed by Fitch et al. [3, 4] have been integrated in the Weather Research and Forecasting (WRF) model to mimic wind farms on larger domains with coarser resolution. These parameterizations are restricted to grid cell size of 1 km or larger due to the implementation of the turbulent kinetic energy production of the wind turbines into the planetary boundary layer scheme. These resolutions may not suffice for the study of wake interactions, as multiple turbines may be located on the same computational

To have a better description of the turbines, a generalized actuator disk model (GAD) has been implemented into the Weather Research and Forecasting - Large Eddy simulations (WRF-

Content from this work may be used under the terms of the Creative Commons Attribution 3.0 licence. Any further distribution of this work must maintain attribution to the author(s) and the title of the work, journal citation and DOI.

doi:10.1088/1742-6596/1037/6/062010

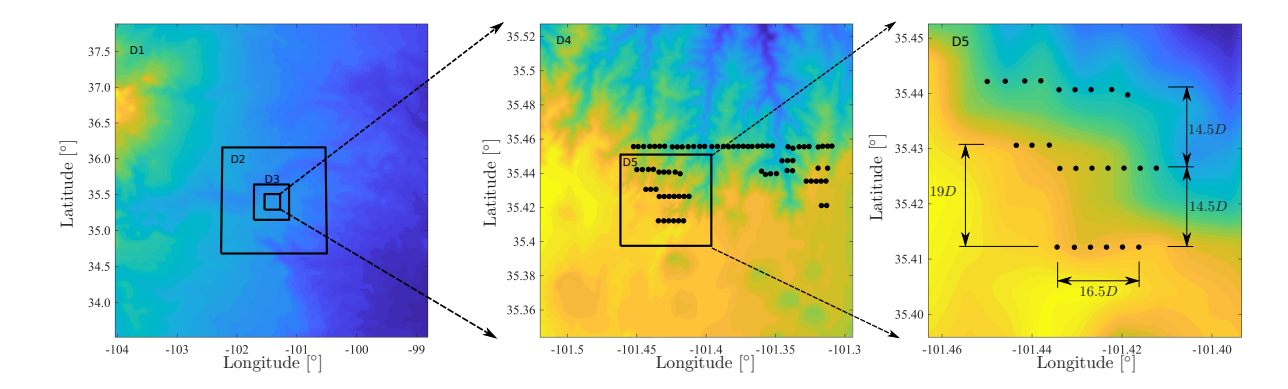


Figure 1. Color contours of the topographic elevation of the Texas Panhandle region. The WRF domains are delimited by the solid lines (——) and the position of each turbine is marked by a solid circle (•).

LES) framework [5]. This study was limited to a single turbine under a fixed surface heat flux, therefore constant wind conditions. Another approach is to use numerical weather prediction (NWP) models to simulate the changing weather conditions and provide large-scale variability to a Large Eddy simulation (LES) with the actuator disk model (ADM) [6, 7]. This is done by averaging the results from the NWP (momentum, temperature and humidity) along the horizontal directions to provide the large-scale forcing along the vertical direction. The LES accurately replicates the wind conditions of the atmospheric boundary layer and also obtains an accurate wake description in comparison to LiDAR measurements. Nevertheless, due to the horizontal averaging of the input wind conditions from the mesoscale simulations and the cyclic boundary conditions, the LES is unable to include structures due to the topography or nearby wind farms that may be resolved by the weather prediction model.

To overcome this limitation, we have combined the Weather Research and Forecasting model with our in-house LES code. A wind farm in north Texas has been modeled with 5 nested domains in WRF. In addition, another simulation with a finer grid has been performed with our in-house LES code. The inlet boundary condition was taken from a section of the innermost domain in WRF. The wind conditions in time and space from WRF are used as inflow condition to our in-house LES code along with radiative boundary condition at one of the boundaries of the domain. The turbines in WRF are modeled as in Fitch et al. [3] while in our LES in-house code they are modeled using the rotating actuator disk [8, 9]. Numerical results are compared against meteorological, SCADA and LiDAR data [10].

2. Methodology

A wind farm located in north Texas is modeled using the Weather and Research Forecasting model, developed by the National Center of Atmospheric research (NCAR), and our in-house high fidelity code UTD-WF. Boundary conditions for WRF are taken from the North America Mesoscale Forecast system (NAM) with a space resolution of 12 km every 3 hours. The largest domain is of $512 \text{ km} \times 512 \text{ km}$ with a resolution of 4 km. To provide the boundary conditions to our in-house LES code [8], five domains were nested into each other (Figure 1). The grid resolution is increased by a factor of 3 from the parent to the child grid. Along the wall normal direction all the domains are discretized with 100 grid cells stretched to cluster more grid points near the surface. The resolution of the stretched grid is between 7 and 12 m at the rotor region, similarly to Lee et al [11]. Details of the domain size and resolution can be found in table 1.

doi:10.1088/1742-6596/1037/6/062010

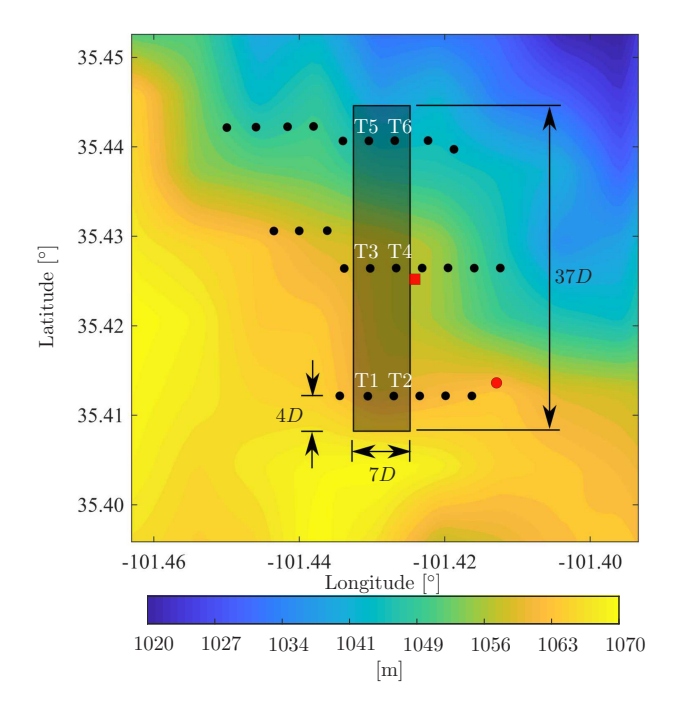


Figure 2. High fidelity Large Eddy simulation domain, delimited by the solid lines (——). The turbines location are indicated by the black circles (•). The location of the meteorological tower is denoted by the red circle (•) and the LiDAR by the red square (•).

For practical applications, resolutions of 1 km require modelling the vertical mixing in the atmospheric boundary layer. Therefore, for domains D1 and D2 the planetary boundary layer (PBL) mixing has been modelled using the Mellor-Yamada, Nakanishi and Niino (MYNN) PBL scheme [12, 13]. For higher resolution domains (D3-D5), the planetary boundary layer scheme has been replaced by fully three-dimensional local sub-grid turbulence (LES) scheme with a turbulent kinetic energy closure.

The wind farm consists of 25 wind turbines of the same manufacturer and model, with a nominal power production of 2.3 MW each, at a rated velocity of $11 \,\mathrm{ms^{-1}}$. The turbines have a rotor diameter, D, of 108 m and a hub height of 80 m with distances between the turbines of 14.5D and 3.3D along the meridional and zonal direction, respectively [10]. The turbines are modeled in the numerical weather prediction code, only in domain D3 through D5, as a momentum deficit and a source of turbulent kinetic energy (TKE) as in Fitch et al.[3]. The TKE production is added to the prognostic equation solved in time for the computation of the turbulent viscosity of the sub-grid stresses.

Table 1. Domains size and resolution						
Domain	Size	Resolution				
D1	$512 \text{ km} \times 512 \text{ km}$	$4~\mathrm{km}$				
D2	$173~\mathrm{km}\times173~\mathrm{km}$	$1.3~\mathrm{km}$				
D3	$58~\mathrm{km} \times 58~\mathrm{km}$	$444 \mathrm{m}$				
D4	$21~\mathrm{km}\times21~\mathrm{km}$	$148 \mathrm{m}$				
D5	$6~\mathrm{km} \times 6~\mathrm{km}$	$49 \mathrm{m}$				
UTD-WF	$4~\mathrm{km}\times756~\mathrm{m}$	$4 \times 6 \text{ m}$				

doi:10.1088/1742-6596/1037/6/062010

An off-line coupling to our LES in-house code is performed for a subset of 6 turbines of the wind farm (Figure 2). The LES code solves the incompressible Navier-Stokes equations discretized in an orthogonal coordinate system using the staggered central second-order finite-difference approximation. Time advancement is performed using a fractional-step method with viscous terms treated implicitly and convective terms explicitly. At each time step, the momentum equations are advanced with the pressure at the previous step, that yields an intermediate non-solenoidal velocity field. A scalar quantity ϕ projects the non-solenoidal field onto a solenoidal one. A hybrid low-storage third-order Runge–Kutta scheme is used to advance the equations in time. Details of the numerical method can be found in Orlandi et al. [14]. The turbines are modelled using the rotating actuator disk model and are controlled with an adapted version of the baseline controller in Laks et al.[15] to adjust the generator torque, blade pitch angle and yaw orientation. The angular velocity of the turbine is determined by the rotor dynamics, balancing the aerodynamic and generator torque. The tower and nacelle of the turbines are modelled using the immersed boundary method that has been widely validated [16, 2].

The computational domain is 37D and 7D along the meridional and zonal direction, respectively, and 10D along the vertical direction (Figure 2). Because the wind direction is predominantly from south-east and south-west, inflow conditions are given by the velocity in a plane located 4D from the southern-most row of turbines obtained from domain D5 of the WRF simulation with a time resolution of one minute. Neutral atmospheric conditions are kept in the high fidelity LES code. Radiative boundary conditions are imposed at the northern-most boundary and periodic conditions along the zonal direction.

The WRF and UTD-WF simulations were performed in our in-house cluster using a total of 128 and 64 Intel Xeon (Sandy Bridge) cores, respectively. Best performance was found from hybrid distributed and shared memory parallel capabilities of the WRF code. The ratio of the wall-clock time to simulation integration time is approximately 3 for WRF and 6.6 for our inhouse code (the grid has about twice the grid points and finer time integration than WRF). We recall that the simulations are not in sync, the coupling is one-way, therefore, the computational time of one domain is not affected by the other domains.

3. Results and analysis

3.1. WRF Results

An assessment of the WRF results has been performed by comparing the wind speed and direction with met-tower measurements. The location of the met-tower is shown in Figure 2. The wind velocity and direction are taken at the hub height (80 m above the ground), as a 10 minutes average. During the evening transition, from convective to stable atmospheric condition, it is observed an increase in the wind speed and a decrease in the fluctuations compared to the day-time period (Figure 3a). Furthermore, the wind direction changes from south-east during the night-time to south-west during the day-time (Figure 3b). The wind speed and direction obtained with the domain D5 agree well with met-tower data. Changes in the variability from the stable to convective boundary layer are also well captured.

To provide a quantitative comparison between the met-tower measurements and the WRF simulation the mean absolute gross error is computed as

$$MAGE = \frac{1}{N} \sum_{i=1}^{N} |P - M|,$$
 (1)

where P and M are the wind speed or wind direction of the numerical simulation and the measurements, respectively, and N is the total amount of data compared. The wind speed and wind direction have a mean absolute gross error of $1.0 \,\mathrm{ms}^{-1}$ and 9.5° , respectively. To evaluate

doi:10.1088/1742-6596/1037/6/062010

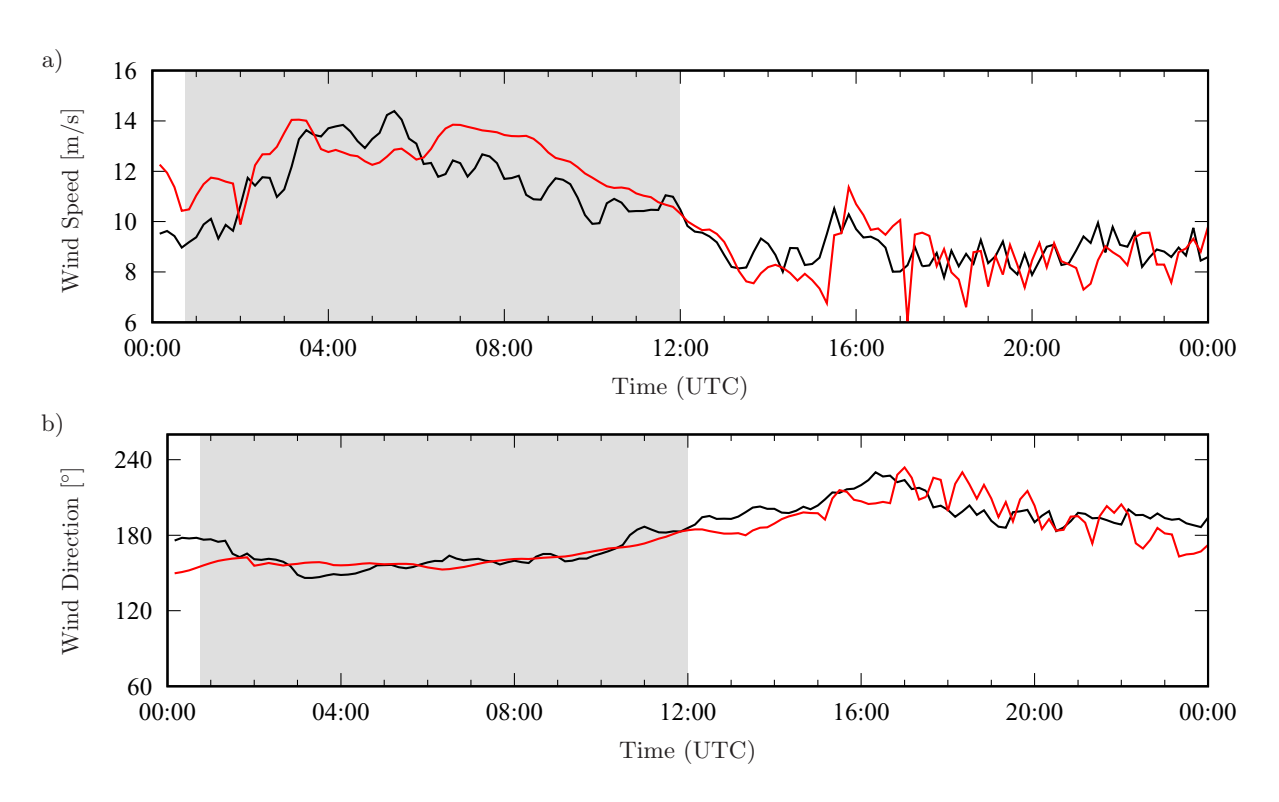


Figure 3. Time series of the wind speed (a) and wind direction (b) at 80 m height from the meteorological tower (\longrightarrow) and WRF simulation on domain D5 (\longrightarrow). The shaded region delimits the night-time period.

the variability of the numerical simulation with respect to the measurements as well as the difference between the mean values, the Willmott's index of agreement [17] (ρ) is computed as

$$\rho = 1 - \frac{\sum (P - M)^2}{\sum \left[|P - \overline{M}| + |M - \overline{M}| \right]^2},\tag{2}$$

where the overline indicates the time average. The wind speed and wind direction have an index of agreement of 90% and 92%, respectively.

Variations of the wind speed and direction are mostly driven by the atmospheric stability. To characterize the atmospheric boundary layer stability, the Bulk Richardson number, Ri_B , is computed as

$$Ri_B = \frac{g\Delta\theta_v\Delta y}{\theta_v\left(\Delta U^2 + \Delta W^2\right)},\tag{3}$$

where θ_v is the virtual potential temperature, g is the gravitational acceleration, y is the height of the measurement and U and W are the horizontal velocity components. The Δ stands for the height difference at which the measurements were taken, 36 m and 80 m.

Night-time is characterized by a stable atmospheric condition, $Ri_B > 0$, where the turbulence production is dominated by the shear (Figure 4). In contrast, an unstable atmospheric condition is observed during day-time, where the buoyancy driven turbulence production is caused by the incident heat radiation. The effects of the atmospheric stability are also reflected on the velocity profile due to the mixing in the atmospheric boundary layer [18]. The wind speed shear exponent, α , is computed as

$$U_H(y) = U_R \left(\frac{y}{y_R}\right)^{\alpha},\tag{4}$$

doi:10.1088/1742-6596/1037/6/062010

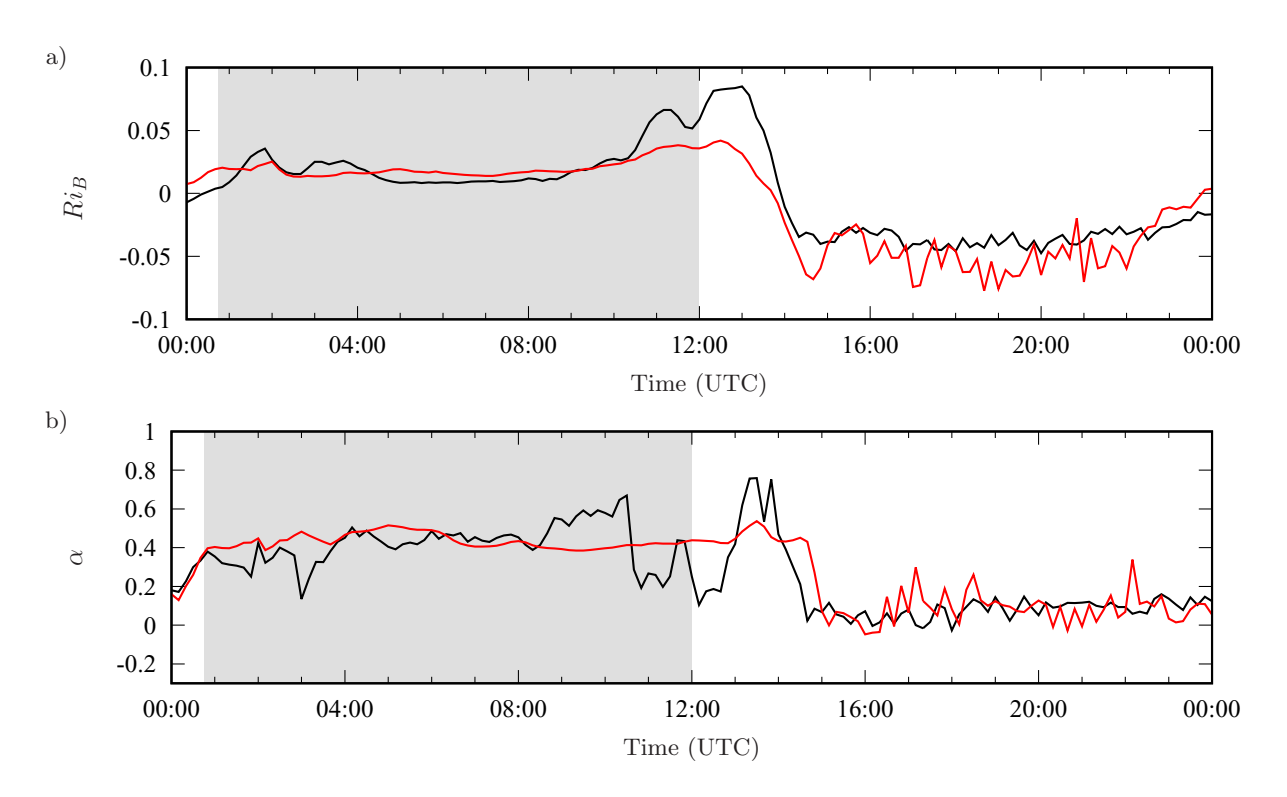


Figure 4. Time series of the bulk Richardson number Ri_B (a) and wind shear exponent α (b) computed from the meteorological tower (——) and WRF D5 simulation (——). The shaded region delimits the night-time period.

where U_H is the mean horizontal wind speed, U_R is the mean horizontal wind speed at a reference height y_R (Figure 4b). As the mixing increases due to buoyancy driven turbulence during the unstable atmospheric condition, it is observed a wind shear exponent $\alpha < 0.2$. During stable atmospheric condition, night-time, the turbulent mixing is lower than during convective condition, therefore the wind speed shear exponent increases to $\alpha > 0.3$.

The bulk Richardson number, Ri_B , obtained numerically with WRF with D5 resolution has a mean absolute gross error and index of agreement of 0.01% and 93%, respectively. The wind shear exponent, which is essential to compute the power production of the turbines, has a MAGE of 9% and ρ of 88% for the presented diurnal cycle.

3.2. UTD-WF LES Results

A comparison between the LiDAR measurements [10], WRF and UTD-WF numerical results is shown in Figure 5 for both stable (a-e) and unstable (f-j) conditions. Reconstructing the LiDAR measured velocity into Cartesian components may introduce errors due to the assumption of homogeneity [19]. To avoid this source of uncertainty, especially near the turbine wake, the wind velocity field of WRF and UTD-WF is computed as in the unprocessed LiDAR measurements (Figure 5a-c,f-h). This consists in projecting the wind velocity onto a conical surface, with center at the LiDAR position (Figure 2). Because the beam of the LiDAR measures the wind speed in its line of sight (LOS), no information about its perpendicular component is provided. Thus, the LiDAR measurements show a zero velocity band near the center row of turbines. Wind speed on an horizontal plane at hub-height obtained from the numerical simulations (Figure 5 d-e,i-j) is shown for comparison against the absolute radial velocity counter part. The wind speed at hub-height is similar to the radial velocity counterpart with the exception of the region where the

doi:10.1088/1742-6596/1037/6/062010

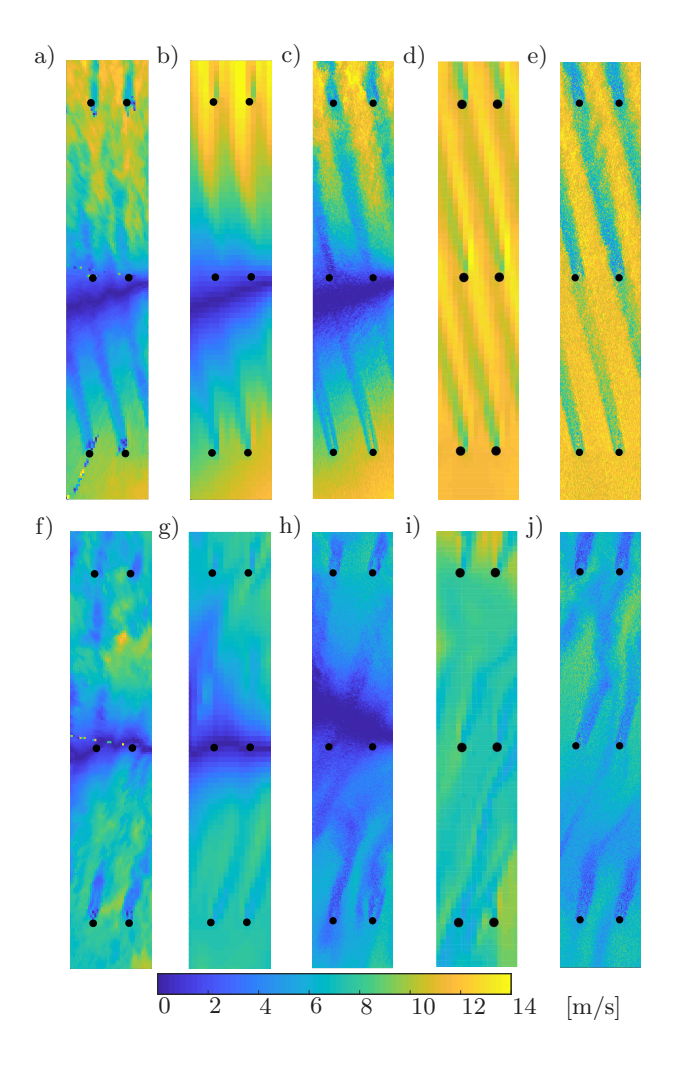


Figure 5. Color contours of the absolute value of the radial velocity field obtained from the LiDAR measurements (a,f), WRF (b,g) and UTD-WF LES (c,h) during stable (a-e) and unstable (f-j) atmospheric conditions at an elevation angle of 3° . The velocity magnitude obtained from WRF (d,i) and UTD-WF (e,j) on a plane at hub-height is alsow shown as reference. The turbine positions are denoted by a black circle (\bullet) .

velocity is perpendicular to the LOS. Wake interaction between the turbine is observed as the wake of the turbines on the first row impinges on the rotor of the turbine in the central row during stable atmospheric condition (Figure 5a-c). The periodic conditions on the lateral boundaries of the high fidelity LES approximate to a good degree the wake of the adjacent columns of turbines within the wind farm. The momentum deficit in the wake of the WRF simulation is slightly under-predicted in comparison to the LiDAR measurements and the LES results. The direction of the wake of WRF, UTD-WF and LiDAR agree well. The momentum deficit in the turbine wake obtained with the high fidelity LES is closer to the LiDAR measurements than that obtained with WRF domain D5 resolution. In fact, the wake obtained with WRF, during stable condition, expands more than the LiDAR measurements and the numerical results obtained with UTD-WF.

Due to the mixing and entrainment of mean kinetic energy, during convective atmospheric conditions (Figure 3f-h) the wake is shorter than during stable condition. Despite our LES code at the moment does not solve the energy equation, the velocity profile and fluctuations imposed

doi:10.1088/1742-6596/1037/6/062010

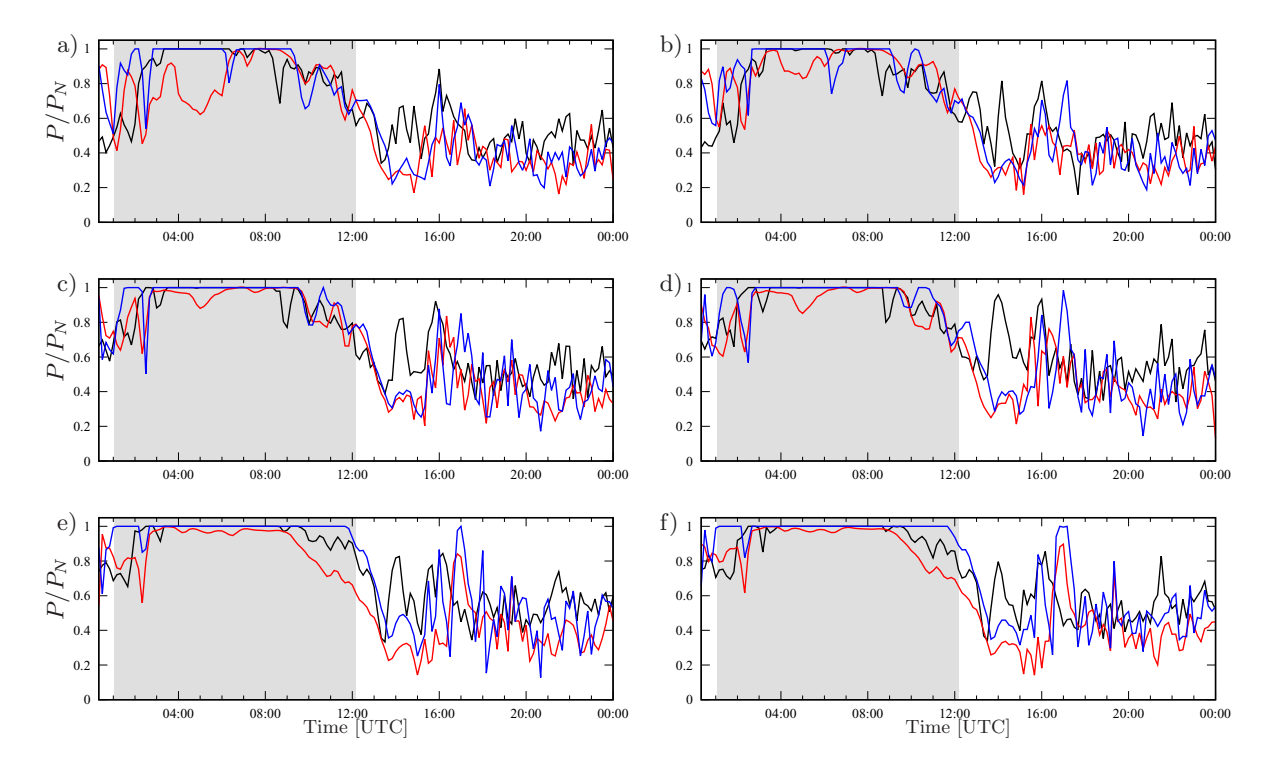


Figure 6. Power production normalized with the rated power, P_N , of the northern-most row (a,b), middle row (c,d) and southern-most row (e,f) of turbines; (——) SCADA measurements, (——) WRF simulation and (——) high-fidelity LES. The night-time is delimited by the shaded region.

at the inlet from the WRF solution of domain D5 allow a close representation of the flow with respect to LiDAR measurements.

To evaluate the accuracy of the numerical results, the power production is compared against the supervisory control and data acquisition (SCADA) system (Figure 6). Because the wind velocity during stable condition is above the manufacturer rated speed, all the turbines operate in region 3, reaching nominal power production during the night-time. As the wind velocity decreases and the buoyancy generated turbulence dominates, the power production of the turbines decreases to about 50% and, consequently, the fluctuations of power production increase.

A noticeable difference between WRF and UTD-WF is observed on turbines T1 and T2 in the southern-most row (see Figure 2), during the morning transition (Figure 6e,f). The velocity profiles upstream of turbine T1 obtained by UTD-WF and WRF are very similar as shown in Figure 7a. Small fluctuations in the velocity profile obtained with UTD-WF are due to the higher resolution of the computational grid, that is capable of capturing fluctuations at a smaller scale than WRF. The momentum deficit at the location of the rotor is similar in WRF and UTD-WF (Figure 7b). Further downstream, 0.5D downstream the turbine rotor (Figure 7c), the ADM causes a larger momentum deficit than that of WRF. This difference in the momentum deficit could not be observed at the rotor because the force of the rotating actuator disk is spread over four grid points along the streamwise direction to avoid discontinuities in the discretization of the Navier-Stokes equation [9]. On the other hand, the turbine model implemented in WRF is designed for numerical grids with very low resolution. It computes the power production of each turbine using the manufacturer power curve and the velocity at hub height at the location of the turbine. Due to the induction zone and coarse grid resolution, the reference velocity used

doi:10.1088/1742-6596/1037/6/062010

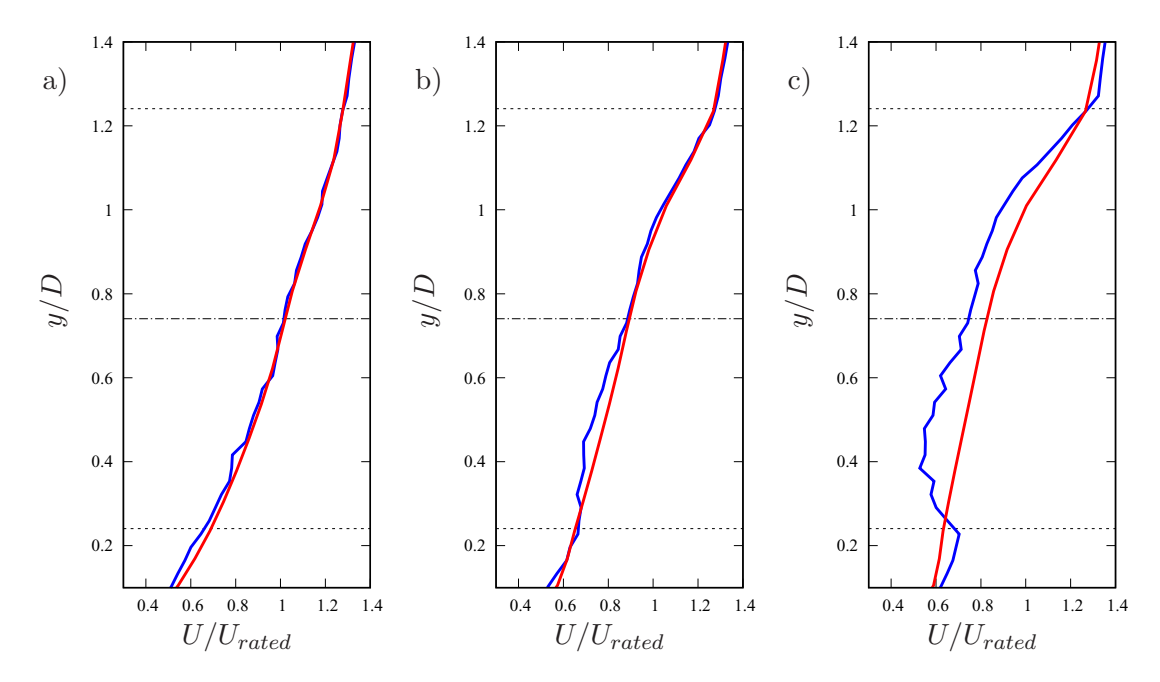


Figure 7. Velocity profile at 10:30 UTC averaged along 1D in the spanwise direction; a) 2D upstream, b) at the rotor and c) 0.5D downstream of turbine T1 of the WRF simulation (——) and high-fidelity LES (——). The rotor region is delimited by (·······) and the hub-height is indicated with ($-\cdot$ —).

in the model may be slightly smaller than the upstream wind speed. As a consequence the power production estimated with the model and the momentum deficit are under-predicted. In addition, using only the velocity at hub-height may also under-estimate the power production especially if the velocity profile presents a high shear across the rotor of the turbine. This is not the case with the actuator disk model. For the rotating actuator disk, the power is computed from the integral of the aerodynamic forces in each blade section. Therefore, it accounts for the heterogeneity of wind speed (and the angle of attack) due to the high shear.

Despite this difference in the computation of the power production, both sets of simulations have good agreement with the SCADA data. The power production of each turbine, computed by WRF and UTD-WF, presents a mean absolute gross error of about 14% and 12%, respectively (table 2). Similarly, both models show a very good index of agreement with UTD-WF results showing a small improvement in the predicted power.

Table 2. Turbine power production mean absolute gross error and index of agreement

MAGE		ho		
Turbine	WRF	UTD-WF	WRF	UTD-WF
T1	0.15	0.11	0.83	0.87
T2	0.13	0.11	0.85	0.88
T3	0.12	0.11	0.88	0.88
T4	0.13	0.13	0.84	0.84
T5	0.16	0.12	0.80	0.88
T6	0.13	0.12	0.88	0.90

IOP Conf. Series: Journal of Physics: Conf. Series 1037 (2018) 062010 doi:10.1088/1742-6596/1037/6/062010

4. Conclusion

Numerical simulations of the flow in a wind farm in the north Texas region have been performed by combining 5 nested domains in WRF with our in-house LES code (UTD-WF) for a single diurnal cycle. Turbines in WRF are modeled as a momentum deficit and a source of turbulent kinetic energy as in Fitch et al. [3, 4], while a Rotating Actuator Disk is used in UTD-WF. The wind speed and wind direction of the innermost WRF domain are used to provide time and space resolved boundary conditions to our in-house LES code. Wind speed, direction, power production, bulk Richardson number and the wind speed shear exponent obtained in the innermost domain of WRF (with $50\,m$ resolution) agree well with met-tower, LiDAR and SCADA measurements.

Simulations performed with our in-house LES code improve slightly the results because of a finer grid (4×6 m resolution) and a more detailed turbine model, the RADM, which accounts for the variability of the wind speed in the rotor when the shear is high. However, both numerical codes provide a good approximation of the power production of the turbines. The index of agreement obtained with WRF and UTD-WF is 85% and 88%, respectively.

Despite the simulation wall-clock time is around 3 and 6 times the numerical integration time, present results are promising. By increasing the number of processors and optimizing the parallelization, LES may be used in the near future as a valuable tool for the design and analysis of wind farms.

Acknowledgments

The authors wish to acknowledge Luis Martínez-Tossas and Matthew Churchfield for useful discussion. The present work was supported by the National Science Foundation grant no.1243482 (the WINDINSPIRE project). The Texas Advanced Computing Center (TACC) is acknowledged for providing computational resources.

References

- Martínez-Tossas L A, Churchfield M J and Meneveau C 2017 Wind Energy 20 1083–1096 ISSN 1099-1824 we.2081
- [2] Santoni C, Carrasquillo K, Arenas-Navarro I and Leonardi S 2017 Wind Energy 20 1927–1939
- [3] Fitch A C, Olson J B, Lundquist J K, Dudhia J, Gupta A K, Michalakes J and Barstad I 2012 Monthly Weather Review 140 3017–3038
- [4] Fitch A C, Olson J B and Lundquist J K 2013 Journal of Climate 26 6439-6458
- [5] Mirocha J D, Kosovic B, Aitken M L and Lundquist J K 2014 Journal of Renewable and Sustainable Energy 6 013104
- [6] Vollmer L, Steinfeld G and Kühn M 2017 Wind Energy Science 2 603-614
- [7] Vollmer L, Lee J C Y, Steinfeld G and Lundquist J K 2017 Journal of Physics: Conference Series 854 012050
- [8] Santoni C, Ciri U, Rotea M and Leonardi S 2015 2015 American Control Conference (ACC) (IEEE)
- [9] Ciri U, Petrolo G, Salvetti M V and Leonardi S 2017 Energies 10 ISSN 1996-1073
- [10] El-Asha S, Zhan L and Iungo G V 2017 Wind Energy 20 1823–1839 ISSN 1099-1824 we.2123
- [11] Lee J C Y and Lundquist J K 2017 Geoscientific Model Development 10 4229-4244
- [12] Nakanishi M and Niino H 2006 Boundary-Layer Meteorology 119 397–407 ISSN 1573-1472
- [13] Nakanishi M and Niino H 2009 Journal of the Meteorological Society of Japan. Ser. II 87 895-912
- [14] Orlandi P and Leonardi S 2008 Journal of Fluid Mechanics 606 399415
- [15] Laks J H, Pao L Y and Wright A D 2009 Proceedings of the American Control Conference 2096–2103 ISSN 0743-1619
- [16] Orlandi P and Leonardi S 2006 Journal of Turbulence 7 N73
- [17] Willmott C J 1981 Physical Geography 2 184–194
- [18] Wharton S and Lundquist J K 2012 Wind Energy 15 525-546 ISSN 1099-1824
- [19] Lundquist J K, Churchfield M J, Lee S and Clifton A 2015 Atmospheric Measurement Techniques 8 907–920